Limit-Induced Stable Limit Cycles in Power Systems

Patel Bhageerath Reddy Ian A. Hiskens
Department of Electrical and Computer Engineering
University of Wisconsin - Madison
Madison WI 53706 USA

***Abstract*— Heavily loaded power systems are susceptible to Hopf bifurcations, and consequent oscillatory instability. The onset of instability can be predicted by small disturbance (eigenvalue) analysis, but the ensuring behaviour may depend strongly on nonlinearities within the system. In particular, physical limits place bounds on the divergent behaviour of states. This paper explores the situation where generator field-voltage limits capture behaviour, giving rise to a stable (though non-smooth) limit cycle. It is shown that shooting methods can be adapted to solve for such non-smooth limit-induced limit cycles. By continuing branches of limit-induced and smooth limit cycles, the paper established the co-existence of equilibria, smooth and non-smooth limit cycles. Furthermore, it is shown that when branches of limit-induced and smooth limit cycles merge, the limit cycles are annihilated at a grazing bifurcation.**

***Index Terms*— Limit cycles, piecewise smooth dynamics, hybrid systems, shooting methods, Hopf bifurcations, continuation methods.**

I. Introduction

Automatic voltage regulators (AVRs), coupled with power system stabilizers (PSSs), play a fundamental role in the dynamical behaviour of power systems. A simple example of an AVR/PSS/exciter model [1] is provided in Figure 1. To achieve good voltage regulation, the AVR gain K_A should have a high value. However it is well known that as K_A increases, a Hopf bifurcation may occur at a critical value K_A^*, resulting in the system equilibrium point losing local stability [2].

Local stability properties are well described by small disturbance analysis, where the nonlinear system equations are linearized about the equilibrium point. At a Hopf bifurcation, a conjugate pair of eigenvalues of the linearized system migrate across the imaginary axis. Such bifurcations may be either subcritical or supercritical [3]. In the former case, when $K_A < K_A^*$, the stable equilibrium point generically coexists with an unstable limit cycle. At $K_A = K_A^*$, this limit cycle merges with the equilibrium point, resulting in an unstable equilibrium point for $K_A > K_A^*$. In the latter case, when $K_A > K_A^*$, a stable limit cycle coexists with the unstable equilibrium point. The limit cycle and equilibrium point merge at $K_A = K_A^*$, with no limit cycle existing (locally) for $K_A < K_A^*$.

Many systems, including power systems, have limiters that place restrictions on large excursions of state variables. This is illustrated in the AVR/PSS/exciter model of Figure 1. The PSS output V_{PSS} is limited by clipping limits, whilst the field voltage E_{fd} is restricted by non-windup limits [4]. Small disturbance stability assessment cannot predict the effects of such limits.

Research supported by the National Science Foundation through grant ECS-0332777.

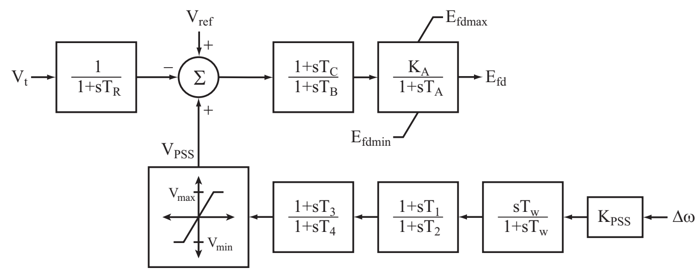

Fig. 1. Simple PSS/AVR/exciter model.

It has been shown previously [5], [6] that stable limit cycles may be induced by state limits. Furthermore, these *limit-induced* limit cycles can coexist with other stable and unstable attractors, for values of K_A both above and below K_A^*. However prior investigations have been restricted by a lack of numerical methods for directly locating non-smooth limit cycles. Such techniques have recently been established in [7], [8]. This paper exploits these newer numerical techniques to further explore limit-induced limit cycles.

The paper is organized as follows. A generic dynamic model is introduced in Section II, along with trajectory sensitivity concepts. Section III provides background to limit cycle analysis, and an example is explored in Section IV. Conclusions are presented in Section V.

II. System Dynamic Behaviour

A. Model

The dynamical behaviour of continuous-time systems, such as power systems, can be expressed in terms of the *flow*,

$$x(t) = \phi(x_0, t), \tag{1}$$

which describes the evolution of dynamic states x over time, starting from the initial condition $x(t_0) = x_0$. In general, ϕ cannot be expressed in closed form, and so must be obtained by numerical integration [9].

The flow may well describe behaviour that involves interactions between continuous dynamics and discrete events [10].

Systems that exhibit such behaviour are known as *hybrid* or *piece-wise smooth* dynamical systems. Power systems exemplify such systems. Referring to the AVR/PSS of Figure 1, an event occurs when V_{PSS} or E_{fd} encounters a limit. The outcome of such an event is a change in the description of subsequent system behaviour.

Along smooth sections of the flow, away from events, dynamics are driven by the tangent vector field

$$\dot{x} = \frac{\partial \phi}{\partial t} \equiv f. \tag{2}$$

At an event, the tangent vector field f may switch and/or the state undergo a reset

$$x^+ = h(x^-), \tag{3}$$

where x^- and x^+ refer to the pre- and post-event values of x respectively. (The event is assumed to take zero time.)

For power systems, the dynamic states must generally satisfy algebraic constraints,

$$g(x, y) = 0 \tag{4}$$

that introduce algebraic variables y. However it will be assumed that the Jacobian $D_y g$ is globally nonsingular, effectively allowing the elimination of y. Therefore, for notational clarity, (4) will be disregarded in later analysis.

This model is a simplification of a more complete hybrid system model presented in [10], [11]. This simplification favours clearer development of limit cycle analysis. However, details of the full model can be found in [8].

B. *Trajectory sensitivities*

Algorithms for locating limit cycles require the sensitivity of a trajectory (flow) to perturbations in initial conditions [12]. To obtain the sensitivity of the flow ϕ to initial conditions x_0, the Taylor series expansion of (1) is formed. Neglecting higher order terms gives

$$\Delta x(t) = \frac{\partial \phi(t)}{\partial x_0} \Delta x_0 \equiv \Phi(x_0, t) \Delta x_0 \tag{5}$$

where Φ is the *sensitivity transition matrix*, or *trajectory sensitivities*, associated with the x flow [13]. Equation (5) describes the change $\Delta x(t)$ in a trajectory, at time t along the trajectory, for a given (small) change in initial conditions Δx_0.

Space limitations preclude the inclusion of the variational equations describing the evolution of Φ. Full details are given in [10], [11]. It should be emphasized that Φ does not require smoothness of the underlying flow ϕ. Trajectory sensitivities are well defined for the non-smooth and/or discontinuous flows associated with realistic power systems.

Furthermore, the computational burden of generating Φ is minimal. It is shown in [11], [14], [15] that when an implicit numerical integration technique such as trapezoidal integration is used, trajectory sensitivities can be obtained as a by-product of computing the underlying trajectory.

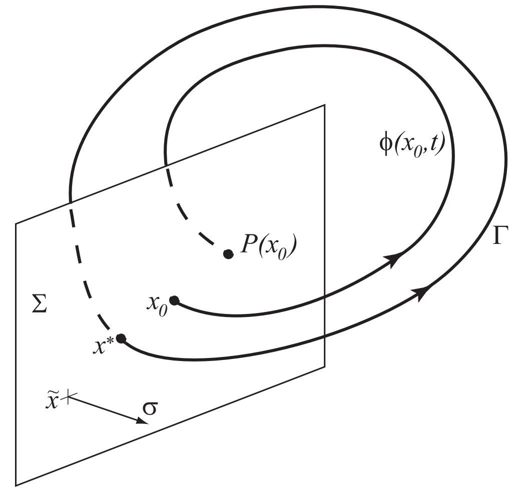

Fig. 2. Poincaré map.

III. Limit Cycle Analysis

A. *Poincaré maps*

Limit cycles and their stability can be determined using Poincaré maps [3], [16]. This section provides a brief review of these concepts, and establishes a connection with trajectory sensitivities.

A Poincaré map effectively samples the flow of a periodic system once every period. The concept is illustrated in Figure 2. If the limit cycle is stable, oscillations approach the limit cycle over time. The samples provided by the corresponding Poincaré map approach a fixed point. An unstable limit cycle results in divergent oscillations. For such a case the samples of the Poincaré map diverge.

To define a Poincaré map, consider the limit cycle Γ shown in Figure 2. Let Σ be a hyperplane transversal to Γ and defined by

$$\Sigma = \{x : \sigma^T (x - \tilde{x}) = 0\} \tag{6}$$

where $\tilde{x}$ is a point anchoring Σ, and σ is a vector normal to Σ. The trajectory emanating from x^* will again encounter Σ at x^* after T seconds, where T is the minimum period of the limit cycle. Due to the continuity of the flow ϕ with respect to initial conditions, trajectories starting on Σ in a neighbourhood of x^* will, in approximately T seconds, intersect Σ in the vicinity of x^*. Hence ϕ and Σ define the Poincaré map

$$x_{k+1} = P(x_k) := \phi(x_k, \tau_r(x_k)). \tag{7}$$

where $\tau_r(x_k) \approx T$ is the time taken for the trajectory to return to Σ. Complete details can be found in [3], [16].

B. *Shooting method*

From (7), it can be seen that a point x^* on the limit cycle can be located by using Newton's method to solve the nonlinear algebraic equations

$$F_l(x^*) = \phi(x^*, \tau_r(x^*)) - x^* = 0. \tag{8}$$

The solution process therefore has the iterative form

$$x^{i+1} = x^i - \left(DF_l(x^i)\right)^{-1} F_l(x^i). \tag{9}$$

It is shown in [8] that the Jacobian DF_l is given by

$$DF_l(x^i) = \left(I - \frac{f|_{\tau_r(x^i)}\sigma^T}{\sigma^T f|_{\tau_r(x^i)}} \right) \Phi(x^i, \tau_r(x^i)) - I \qquad (10)$$

where f is given by (2). Notice that because the flow ϕ and associated sensitivities Φ are well defined for non-smooth systems, solution of (8) is also well defined for such systems.

It can be seen from (8) that evaluation of $F_l(x^i)$ at each iteration requires numerical integration. This process is therefore referred to as a *shooting method* [12].

C. Limit cycle stability

Stability of the Poincaré map (7) is determined by linearizing P at the fixed point x^*, i.e.,

$$\Delta x_{k+1} = DP(x^*)\Delta x_k. \qquad (11)$$

From the definition of $P(x)$ given by (7), it follows that

$$DP(x^*) = \left(I - \frac{f|_{x^*}\sigma^T}{\sigma^T f|_{x^*}} \right) \Phi(x^*, T) \qquad (12)$$

where $\tau_r(x^*) = T$.

The matrix $\Phi(x^*, T)$ is exactly the trajectory sensitivity matrix after one period of the limit cycle, i.e., starting from x^* and returning to x^*. This matrix is called the *Monodromy matrix*. It is shown in [16] that for an autonomous system, one eigenvalue of $\Phi(x^*, T)$ is always 1, and the corresponding eigenvector lies along $f|_{x^*}$. The remaining eigenvalues of $\Phi(x^*, T)$ coincide with the eigenvalues of $DP(x^*)$, and are known as the *characteristic multipliers* m_i of the periodic solution. The characteristic multipliers are independent of the choice of cross-section Σ.

Because the characteristic multipliers m_i are the eigenvalues of the linear map $DP(x^*)$, they describe the (local) stability of the Poincaré map $P(x_k)$. Hence the (local) stability of the periodic solution is determined by:

1) All m_i lie within the unit circle, i.e., $|m_i| < 1, \forall i$. The map is stable, so the periodic solution is stable.
2) Some m_i lie outside the unit circle. The periodic solution is unstable.

Interestingly, there exists a particular cross-section Σ^*, such that

$$DP(x^*)\zeta = \Phi(x^*, T)\zeta \qquad (13)$$

where $\zeta \in \Sigma^*$. This cross-section Σ^* is the hyperplane spanned by the $n-1$ eigenvectors of $\Phi(x^*, T)$ that are not aligned with $f|_{x^*}$. Therefore the vector σ^* that is normal to Σ^* is the left eigenvector of $\Phi(x^*, T)$ corresponding to the eigenvalue 1. The hyperplane Σ^* is invariant under $\Phi(x^*, T)$, i.e., $\Phi(x^*, T)$ maps vectors $\zeta \in \Sigma^*$ back into Σ^*.

D. Continuation methods

It is often useful to explore the changes in limit cycle structure and stability properties that result from parameter variations. This can be achieved by introducing a free parameter θ into (8), giving

$$F_l(x^*, \theta) = 0. \qquad (14)$$

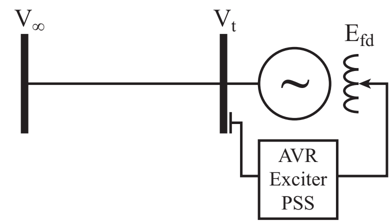

Fig. 3. Single machine infinite bus system.

As shown earlier, the point x^* given by (8) fully specifies the associated limit cycle. Therefore, the 1-manifold, or curve, defined by (14) describes the variation of x^*, and hence the associated limit cycle variation, with changes in parameter θ.

The curve given by (14) can be traced using a homotopy method [17]. A predictor-corrector process is presented in [8]. Note that even when the underlying dynamic behaviour is non-smooth, curves given by (14) are generally smooth. Curve smoothness may be lost at grazing bifurcations though [8], [18]. The details are beyond the scope of this paper, though an illustration is provided in Section IV.

IV. Example

A. Model

A single machine infinite bus system was used to explore the existence and nature of limit-induced limit cycles. This system is shown schematically in Figure 3, and parameter values are provided in the appendix. The generator was represented by a sixth order machine model [19], and the AVR/exciter by the model given in Figure 1. (The PSS was disabled for these studies.) This resulted in 9 dimensional state space, that is $x \in \mathbb{R}^9$.

The non-windup limits on E_{fd} introduce non-smoothness into the model. It will be shown that these limits restrict growing (unstable) oscillations in a way that gives rise to stable limit cycles.

This example illustrates that the efficient computation of trajectory sensitivities for large-scale non-smooth systems allows, 1) the use of shooting methods for locating limit-induced limit cycles, and 2) assessment of their stability properties.

B. Hopf bifurcation

For the parameter values given in the appendix, a Hopf bifurcation occurs at an AVR gain of $K_A^* = 208.22$. The equilibrium point is unstable for $K_A > 208.22$. To illustrate, for a gain of $K_A = 212$, linearization around the equilibrium point gave an unstable eigenvalue pair of $0.0053 \pm j5.86$. The behaviour of the field voltage E_{fd} is shown in Figure 4. The initial growth in oscillation magnitude reflects the instability of the operating point. But notice that behaviour stabilizes to a limit cycle, from around 70 seconds. This is a consequence of the field voltage encountering its maximum limit $E_{fdmax} = 5.4$.

The shooting method was used to locate this stable limit cycle. Convergence was obtained in 3 iterations, with the $V_t - E_{fd}$ projection of the limit cycle shown in Figure 5.

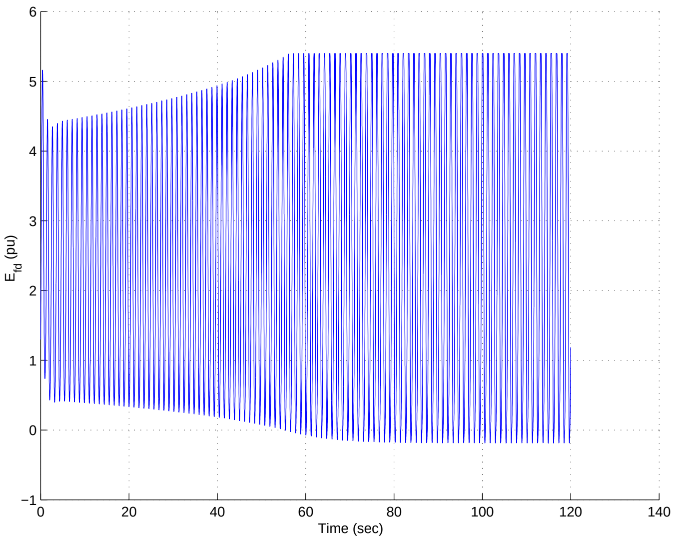

Fig. 4. Response of field voltage E_{fd} for $K_A = 212$.

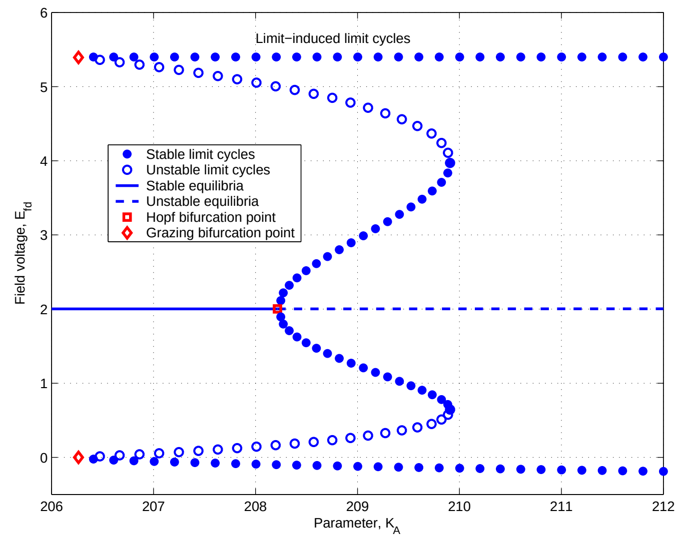

Fig. 6. Bifurcation diagram.

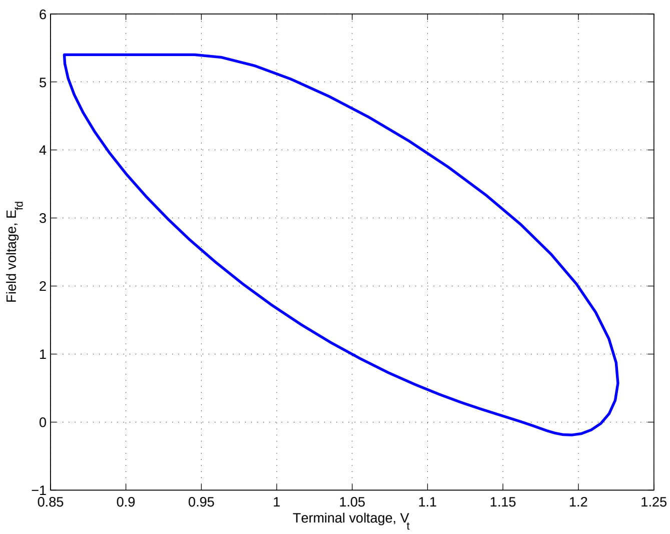

Fig. 5. Stable limit-induced limit cycle for $K_A = 212$.

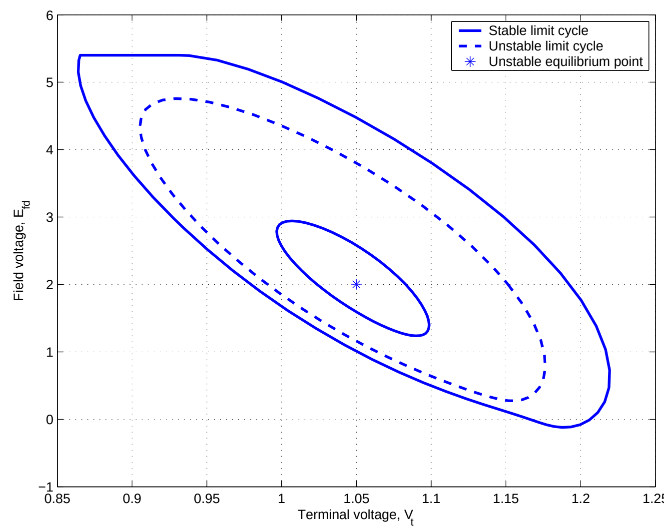

Fig. 7. Co-existing limit cycles and equilibrium point, $K_A = 209$.

It was found that all characteristic multipliers lay within the unit circle, with the largest having a magnitude of 0.83. This confirmed the limit cycle was indeed an attractor.

Further investigation of the Hopf bifurcation revealed that it was in fact supercritical. The bifurcation diagram of Figure 6, produced using the continuation process of Section III-D, shows a branch of stable limit cycles emanating from the Hopf bifurcation.[1] This branch of limit cycles undergoes a cyclic fold at $K_A = 209.9$, beyond which the branch comprises unstable limit cycles.

As shown in Figure 6, the stable non-smooth limit cycles, induced by the E_{fdmax} limit, coexist with the smooth limit cycles that result from the Hopf bifurcation. Over the range $208.22 < K_A < 209.9$, the system exhibits an unstable equilibrium point, an unstable limit cycle, and two stable limit cycles (one smooth and one non-smooth). These limit sets are shown in Figure 7, for a gain $K_A = 209$.

[1]The limit cycles are represented in Figure 6 by the extreme values of E_{fd}.

The shooting method of Section III-B was used to obtain the limit cycles of Figure 7. In all cases, convergence was obtained in three iterations, with each iteration requiring a single simulation of one period of the oscillation. On the other hand, reliance on time-domain simulation would be futile. The unstable limit cycle has characteristic multipliers both inside and outside the unit circle, so time reversal would not achieve convergent behaviour. Furthermore, transient behaviour is poorly damped in the vicinity of the Hopf bifurcation. Therefore lengthy simulation would be required for adequate convergence to the stable limit cycles. Shooting methods are however unaffected by the stability properties and damping associated with a limit cycle.

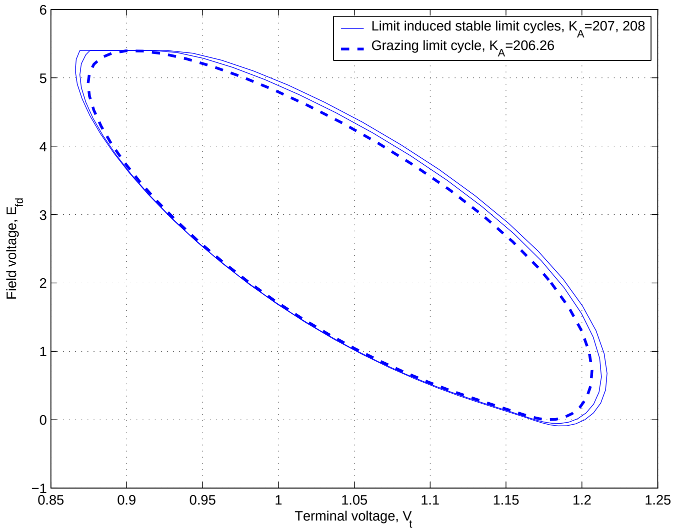

Fig. 8. Grazing limit cycle.

C. Grazing bifurcation

As the gain K_A is reduced, the branches of limit-induced and smooth limit cycles converge, finally merging at $K_A = 206.26$. At that point, the smooth limit cycle becomes tangential to (grazes) the E_{fdmax} limit surface, as shown in Figure 8. Furthermore, the figure shows that as K_A reduces, the limit-induced limit cycle spends less and less time on the limit surface, until it also just grazes that surface. The two limit cycles coalesce at the grazing case. As K_A is further reduced, the limit cycles cannot continue to deform as they did prior to grazing. It follows that the limit cycles must vanish, with structural stability being lost due to a grazing bifurcation [18].

V. Conclusions

Power systems form an important application area within the general class of hybrid (non-smooth) systems. The non-smooth nature of behaviour exhibited by such systems complicates computation and stability analysis of limit cycles. Those complications are overcome through generalization of trajectory sensitivity analysis to non-smooth systems.

Standard Poincaré map results extend naturally to hybrid systems. The Monodromy matrix is obtained by evaluating trajectory sensitivities over one period of the (possibly non-smooth) cyclical behaviour. One eigenvalue of this matrix is always unity. The remaining eigenvalues, i.e., the characteristic multipliers of the periodic solution, determine the local stability properties of the limit cycle.

Restrictions imposed by limiters on state excursions can help prevent instability. For systems that exhibit underlying oscillatory response, limiters tend to induce periodic, (non-smooth) limit cycle behaviour. A case of this form has been explored in the paper. It has been shown that such limit-induced limit cycles can co-exist with other, more traditional, limit sets.

Appendix

The following per unit parameter values fully describe the single machine infinite bus system of Section IV. All parameters are given on a 100 MVA base, with ω in rad/sec.

- Machine parameters: $r_a = 0.0006$, $x_d = 0.588$, $x'_d = 0.0913$, $x''_d = 0.075$, $T'_{d0} = 6.59$, $T''_{d0} = 0.0386$, $x_q = 0.588$, $x'_q = 0.1$, $x''_q = 0.075$, $T'_{q0} = 1.0$, $T''_{q0} = 0.0419$, $x_l = 0.049$, $M = 0.0667$, $D = 0.005$, $T_m = 2.5$.
- AVR parameters: $T_R = 0.04$, $T_A = 0.04$, $T_B = 12$, $T_C = 1$, $V_{setpoint} = 1.05$, $E_{fdmax} = 5.4$, $E_{fdmin} = -5$.
- PSS is disconnected.
- Infinite bus parameters: $V_\infty = 1$.
- Line parameters: $r = 0.01$, $x = 0.25$, $b = 0.4$.

References

[1] IEEE Std 421.5-1992, *IEEE Recommended Practice for Excitation System Models for Power System Stability Studies*, Institute of Electrical and Electronics Engineers, Inc., New York, 1992.

[2] P. Kundur, *Power System Stability and Control*, EPRI Power System Engineering Series, McGraw Hill, 1994.

[3] R. Seydel, *Practical Bifurcation and Stability Analysis*, Springer-Verlag, New York, 2nd edition, 1994.

[4] G. Goodwin, S. Graebe, and M. Salgado, *Control System Design*, Upper Saddle River, New Jersey: Prentice Hall, 2001.

[5] X. Jiang, H. Schattler, J. Zaborszky, and V. Venkatasubramanian, “Hard limit induced oscillations,” in *Proceedings of the IEEE International Symposium on Circuits and Systems*, May 1995.

[6] F. Howell and V. Venkatasubramanian, “Transient stability assessment with unstable limit cycle approximation,” *IEEE Transactions on Power Systems*, vol. 14, no. 2, pp. 667–677, May 1999.

[7] I.A. Hiskens, “Stability of hybrid system limit cycles: Application to the compass gait biped robot,” in *Proceedings of the 40th IEEE Conference on Decision and Control*, Orlando, FL, December 2001.

[8] V. Donde and I.A. Hiskens, “Shooting methods for locating grazing phenomena in hybrid systems,” *International Journal of Bifurcation and Chaos*, 2005, To appear.

[9] L. Shampine, *Numerical Solution of Ordinary Differential Equations*, Chapman and Hall, New York, 1994.

[10] I.A. Hiskens, “Power system modeling for inverse problems,” *IEEE Transactions on Circuits and Systems I: Regular Papers*, vol. 51, no. 3, pp. 539–551, March 2004.

[11] I.A. Hiskens and M.A. Pai, “Trajectory sensitivity analysis of hybrid systems,” *IEEE Transactions on Circuits and Systems I: Fundamental Theory and Applications*, vol. 47, no. 2, pp. 204–220, February 2000.

[12] J. Stoer and R. Bulirsch, *Introduction to Numerical Analysis*, Springer, New York, 2nd edition, 1993.

[13] P.M. Frank, *Introduction to System Sensitivity Theory*, Academic Press, New York, 1978.

[14] W.F. Feehery, J.E. Tolsma, and P.I. Barton, “Efficient sensitivity analysis of large-scale differential-algebraic systems,” *Applied Numerical Mathematics*, vol. 25, pp. 41–54, 1997.

[15] S. Li, L. Petzold, and W. Zhu, “Sensitivity analysis of differential-algebraic equations: A comparison of methods on a special problem,” *Applied Numerical Mathematics*, vol. 32, no. 8, pp. 161–174, 2000.

[16] T.S. Parker and L.O. Chua, *Practical Numerical Algorithms for Chaotic Systems*, Springer-Verlag, New York, NY, 1989.

[17] C.B. Garcia and W.I. Zangwill, *Pathways to Solutions, Fixed Points and Equilibria*, Prentice Hall, Englewood Cliffs, NJ, 1981.

[18] M. di Bernardo, C.J. Budd, and A.R. Champneys, “Grazing and border-collision in piecewise-smooth systems: A unified analytical framework,” *Physical Review Letters*, vol. 86, no. 12, pp. 2553–2556, March 2001.

[19] P.W. Sauer and M.A. Pai, *Power System Dynamics and Stability*, Prentice Hall, Upper Saddle River, NJ, 1998.